

## EVOLUTION OF THE SOLAR ACTIVITY OVER TIME AND EFFECTS ON PLANETARY ATMOSPHERES. I. HIGH-ENERGY IRRADIANCES (1–1700 Å)

IGNASI RIBAS,<sup>1</sup> EDWARD F. GUINAN,<sup>2</sup> MANUEL GÜDEL,<sup>3</sup> AND MARC AUDARD<sup>4</sup>

Received 2004 October 7; accepted 2004 December 9

### ABSTRACT

We report on the results of the Sun in Time multiwavelength program (X-rays to UV) of solar analogs with ages covering  $\sim 0.1$ –7 Gyr. The chief science goals are to study the solar magnetic dynamo and to determine the radiative and magnetic properties of the Sun during its evolution across the main sequence. The present paper focuses on the latter goal, which has the ultimate purpose of providing the spectral irradiance evolution of solar-type stars to be used in the study and modeling of planetary atmospheres. The results from the Sun in Time program suggest that the coronal X-ray–EUV emissions of the young main-sequence Sun were  $\sim 100$ –1000 times stronger than those of the present Sun. Similarly, the transition region and chromospheric FUV–UV emissions of the young Sun are expected to be 20–60 and 10–20 times stronger, respectively, than at present. When we consider the integrated high-energy emission from 1 to 1200 Å, the resulting relationship indicates that about 2.5 Gyr ago the solar high-energy flux was about 2.5 times the present value and about 3.5 Gyr ago was about 6 times the present value (when life supposedly arose on Earth). The strong radiation emissions inferred should have had major influences on the thermal structure, photochemistry, and photoionization of planetary atmospheres and have played an important role in the development of primitive life in the solar system. Some examples of the application of the Sun in Time results on exoplanets and on early solar system planets are discussed.

*Subject headings:* solar-terrestrial relations — stars: activity — stars: chromospheres — stars: coronae — stars: late-type — Sun: evolution

*Online material:* color figures

### 1. INTRODUCTION

The Sun is by far the most important star to us. Without a dependable (stable) star such as the Sun, the Earth would not have developed a rich and diverse biosphere that is home to millions of living species. Because of ever accelerating nuclear reactions in its core, the Sun is a slowly evolving variable star that has undergone a  $\sim 40\%$  increase in luminosity over the last 4.5 Gyr, as predicted by the standard solar evolution model (e.g., Girardi et al. 2000). On much shorter timescales, we know that the Sun is also a magnetic-variable star, with an  $\sim 11$  yr sunspot and activity cycle and a  $\sim 22$  yr magnetic cycle. As predicted by magnetic dynamo theory, the Sun's rotation ( $P_{\text{rot}} \sim 25.5$  days) and convective outer envelope interact to generate magnetic fields (Parker 1970). The magnetic dynamo-generated energy is released in the form of flares and chromospheric, transition region, and coronal radiation. Satellite observations of the Sun show that it undergoes small (0.10%–0.15%) variations in total brightness over its activity cycle, although the changes at short wavelengths (UV to X-rays) are much more pronounced (10%–500%; Lean 1997).

The magnetic activity of the present Sun is feeble relative to other solar-type stars, but magnetic-induced phenomena still have important effects on Earth and the solar system (see Guinan

& Ribas 2002). Thus, the fundamental question of whether the Sun has always been a relatively inactive star or, in contrast, has experienced some periods of stronger magnetic activity has a strong impact on the evolution of the solar system. Compelling observational evidence (Güdel et al. 1997b) shows that zero-age main-sequence (ZAMS) solar-type stars rotate over 10 times faster than today's Sun. As a consequence of this, young solar-type stars, including the young Sun, have vigorous magnetic dynamos and correspondingly strong high-energy emissions. From the study of solar-type stars with different ages, Skumanich (1972), Simon et al. (1985), and others showed that the Sun loses angular momentum with time via magnetized winds (magnetic braking), thus leading to a secular increase of its rotation period (Durney 1972). This rotation slowdown is well fitted by a power law roughly proportional to  $t^{-1/2}$  (e.g., Skumanich 1972; Soderblom 1982; Ayres 1997). Note that the age–rotation period relationship is tighter for intermediate or old stars, whereas young stars (a few times  $10^8$  yr) show a larger spread in rotation periods. In response to slower rotation, the solar dynamo strength diminishes with time, causing the Sun's high-energy emissions also to undergo significant decreases. Comprehensive studies on this subject were published by Zahnle & Walker (1982) and Ayres (1997). The reader is referred to these publications for background information on the upper atmospheres and related high-energy emissions of solar-type stars.

The Sun in Time program was established some 20 years ago (Dorren & Guinan 1994; Guinan & Ribas 2004) to study a sample of accurately selected solar proxies (G0–G5 V stars) with different ages across the electromagnetic spectrum. The primary aims of the program are (1) to test dynamo models of the Sun in which rotation is the only significant variable parameter and (2) to determine the spectral irradiance of the Sun over its main-sequence lifetime. In the present paper we focus on the

<sup>1</sup> Institut d'Estudis Espacials de Catalunya/CSIC, Campus UAB, Facultat de Ciències, Torre C5-parell-2a planta, 08193 Bellaterra, Spain; iribas@ieec.uab.es.

<sup>2</sup> Department of Astronomy and Astrophysics, Villanova University, Villanova, PA 19085; edward.guinan@villanova.edu.

<sup>3</sup> Paul Scherrer Institut, Würenlingen & Villigen, 5232 Villigen PSI, Switzerland; guedel@astro.phys.ethz.ch.

<sup>4</sup> Columbia Astrophysics Laboratory, Columbia University, 550 West 120th Street, New York, NY 10027; audard@astro.columbia.edu.

TABLE 1  
RELEVANT DATA FOR THE STUDIED SUN IN TIME TARGETS

Name	HD	Spectral Type	$d$ (pc)	$N_{\text{H}}$ ( $\text{cm}^{-2}$ )	$T_{\text{eff}}$ (K)	Mass ( $M_{\odot}$ )	Radius ( $R_{\odot}$ )	Sun $R^{\text{a}}$ ( $R_{\odot}$ )	$P_{\text{rot}}$ (days)	Age (Gyr)	Age Indicator
EK Dra.....	129333	G1.5 V	34.0	$\sim 1.5 \times 10^{18}$	5870	1.06	0.95	0.900	2.68	0.1	Local Association, Li
$\pi^1$ UMa.....	72905	G1.5 V	14.3	$\sim 1 \times 10^{18}$	5850	1.03	0.95	0.902	4.90	0.3	UMa group
$\chi^1$ Ori.....	39587	G1 V	8.7	$9 \times 10^{17}$	5890	1.01	0.96	0.902	5.24	0.3	UMa group
$\kappa^1$ Cet.....	20630	G5 V	9.2	$8 \times 10^{17}$	5750	1.02	0.93	0.910	9.21	0.65	$P_{\text{rot}}$ -age relation, $L_{\text{X}}$
$\beta$ Com.....	114710	G0 V	9.2	$\sim 1 \times 10^{18}$	6000	1.10	1.08	0.925	12	1.6	$P_{\text{rot}}$ -age relation
Sun.....	...	G2 V	1 AU	0	5777	1.00	1.00	1.00	25.4	4.6	Isotopic dating
$\beta$ Hyi.....	2151	G2 IV	7.5	$\sim 2 \times 10^{18}$	5774	1.10	1.90	1.10	$\sim 28$	6.7	Isochrones

<sup>a</sup> Radius of the Sun at the same age from the models of Girardi et al. (2000).

latter goal, which has the ultimate purpose of characterizing the evolution of the solar emissions with direct application to the study and modeling of atmospheres of both solar system planets and exoplanets in orbit around solar-type stars. There are a number of aspects within the solar system in which a stronger high-energy flux from the young Sun could have had a critical impact. Through photochemical and photoionization processes, the strong X-ray and UV emissions of the young Sun could have had a major effect on the evolution of the atmospheres, ionospheres, and climates of the terrestrial planets, including the Earth (e.g., Canuto et al. 1982, 1983; Kasting & Catling 2003; Smith et al. 2004). For example, paleoclimatic models of the Earth should account for the higher levels of ionizing and dissociating UV radiation in the past. Even the development of life on Earth (and possibly on Mars) could have been influenced by the larger doses of sterilizing UV radiation expected from the young Sun (see Cockell et al. 2000).

In this paper we present the results of an investigation of the long-term magnetic history of the Sun, focused on the high-energy emissions (below 1700 Å). Basically, we study the chromospheric, transition region, and coronal emissions, associated with high-temperature atmospheric layers. In contrast, the time evolution of the photospheric emissions is already well characterized because these scale with the overall bolometric luminosity. We have used our selected sample of stellar proxies with ages that cover most of the main-sequence lifetime of the Sun. A large number of multiwavelength observations (X-ray, EUV, FUV, and UV, hereafter XUV) of the solar analogs have been collected to fully describe their spectral irradiances as a function of age and rotation. In addition, the major effects that the young Sun's strong XUV radiation may have had on the photoionization, photochemistry, and erosion of paleoplanetary atmospheres are discussed.

## 2. THE SUN IN TIME SAMPLE

A critical element of any study of the evolution of the Sun's irradiance with time is a carefully selected sample of stars to serve as proxies for the Sun with different rotation periods and therefore, different ages. The Sun in Time sample contains nearby single (or widely separated binary) G0–G5 stars that have known rotation periods and well-determined temperatures, luminosities, and metallicities. In addition, we have been able to estimate the stellar ages by using their memberships in clusters and moving groups, rotation period–age relationships, and, for the older stars, fits to stellar evolution models. Comparisons with stellar models predict stellar masses within 10% of  $1 M_{\odot}$ . Although the complete Sun in Time sample contains over 15 solar analogs, we focus here on six stars that have been observed with a variety of high-energy instruments: EK Dra,

$\pi^1$  UMa,  $\chi^1$  Ori,  $\kappa^1$  Cet,  $\beta$  Com, and  $\beta$  Hyi. These solar analogs cover most of the Sun's main-sequence lifetime at approximate ages of 100 Myr, 300 Myr, 650 Myr, 1.6 Gyr, and 6.7 Gyr. Note that we have not used any proxy for the current Sun but the Sun itself. Although there are no full-disk high-resolution spectra of the Sun (as pointed out by Pagano et al. 2004), the data sets described in § 3.5 have sufficient resolution to fulfill the requirements of the present study. If higher resolution data were necessary, a valid alternative would be to use solar twins. For example, 18 Sco is a nearly perfect solar twin (Porto de Mello & da Silva 1997; Hamilton et al. 2003), but few high-energy observations are available because of its relative faintness. The star  $\alpha$  Cen A is slightly more massive than the Sun but yet a good solar twin (Pagano et al. 2004) and has numerous observations. In this case, however, some of the high-energy observations include the emissions from the active K-type companion  $\alpha$  Cen B, which complicates the analysis significantly.

A discussion of each observed target is provided below, and a summary of the relevant stellar data (including those for the Sun) is shown in Table 1. Stellar radii have been estimated from the observed magnitude, distance, and temperature, whereas masses generally follow from evolutionary model calculations. Also given in Table 1 is the estimated value of the solar radius at the corresponding age provided by the stellar models of Girardi et al. (2000).

*EK Dra.*—This is a nearby G1.5 V star that has traditionally been considered among the most active solar analogs in our neighborhood. Its main properties, including an average rotation period of 2.68 days, were reviewed by Strassmeier & Rice (1998) and Messina & Guinan (2003). Evolutionary models of Girardi et al. (2000) yield a slightly supersolar mass and a ZAMS age at the observed temperature, luminosity, and chemical composition (solar) of EK Dra. Montes et al. (2001a, 2001b and references therein) classified EK Dra as a kinematic member of the so-called Local Association or Pleiades moving group (with an estimated age range of 20–150 Myr) but from the observed Li abundance inferred an age younger than the Pleiades cluster. Similar conclusions were drawn by Wichmann et al. (2003), who obtained an upper limit to the age of EK Dra of 50–100 Myr. Here we adopt an age of  $\sim 100$  Myr, which seems to be a good compromise. Note that EK Dra was found to be a radial velocity variable, with a period of about 12.5 yr, by Duquennoy & Mayor (1991). This companion to EK Dra would have a minimum mass below  $0.4 M_{\odot}$  and thus likely be an M-type star. Metchev & Hillenbrand (2004), using adaptive optics, have recently reported the discovery of a companion to EK Dra with a mass of  $0.20_{-0.08}^{+0.30} M_{\odot}$ . It is not yet clear whether these two independently detected low-mass companions are indeed the same. In any case, neither of them is a concern for our studies

since in the wavelength domain of interest they should contribute only a few percent.

$\pi^1$  *UMa*.—This young solar proxy is an active G1.5 V star with a rotation period of about 4.9 days (Messina & Guinan 2003). Gaidos & González (2002) and Ottmann et al. (1998) carried out detailed spectroscopic analyses and determined accurate values for the stellar temperature and metal abundance (compatible with solar). Evolutionary models of Girardi et al. (2000) indicate a mass just a few percent higher than that of the Sun. Kinematic studies such as those of Montes et al. (2001a, 2001b) and King et al. (2003) classify  $\pi^1$  *UMa* as a probable member of the Ursa Major moving group. Although the age of this kinematic group of stars has traditionally been quoted as about 300 Myr (see, e.g., Soderblom & Mayor 1993), recent work by King et al. (2003) suggests an older age of  $500 \pm 100$  Myr on the basis of a number of complementary criteria. Here we prefer to adopt the canonical age of  $\sim 300$  Myr since it stands in much better agreement with our measured high-energy fluxes as discussed below.

$\chi^1$  *Ori*.—This field G1 V star has a rotation period of about 5.2 days (Messina et al. 2001), which is indicative of its young age. Its temperature and metal abundance (slightly subsolar) were determined by Gratton et al. (1996) and Taylor (2003a, 2003b) with very similar results. King et al. (2003) classified  $\chi^1$  *Ori* as a certain member of the Ursa Major moving group, in agreement with a number of previous studies. In accordance with  $\pi^1$  *UMa*, we have adopted an age estimate of  $\sim 300$  Myr. Interestingly,  $\chi^1$  *Ori* is a spectroscopic binary with an orbital period of about 14 yr (Han & Gatewood 2002), which was recently resolved using adaptive optics at Keck by König et al. (2002). These authors were able to determine the dynamical mass of both  $\chi^1$  *Ori* and its companion. Note that, since  $\chi^1$  *Ori* B has a mass of only  $0.15 M_{\odot}$ , its quiescent high-energy emissions are negligibly small compared with those of its much larger primary companion.

$\kappa^1$  *Cet*.—With spectral type G5 V,  $\kappa^1$  *Cet* is the coolest in the sample. Spectroscopic parameters were determined by Gaidos & González (2002), who also estimated slightly supersolar metal content. Its rotation period was reported to be around 9.2 days by Messina & Guinan (2003), in agreement with other determinations. Evolutionary models of Girardi et al. (2000) yield a mass very close to the solar value. In the kinematic study of Montes et al. (2001b)  $\kappa^1$  *Cet* was not flagged as a member of any of the canonical stellar groups but was classified as a young disk star. In the absence of more direct indicators, we estimate the age of  $\kappa^1$  *Cet* from its rotation period and mean X-ray luminosity ( $\log L_X = 28.8$ , where  $L$  is in  $\text{ergs s}^{-1}$ ; Güdel et al. 1997b). Comparison with Hyades stars in the same  $B-V$  interval as  $\kappa^1$  *Cet* reveals that both its rotation period (cf. Radick et al. 1995) and its X-ray luminosity (cf. Barrado y Navascués et al. 1998) are close to the average of the Hyades members. These criteria suggest for  $\kappa^1$  *Cet* an age close to the canonical Hyades age of  $\sim 650$  Myr, which we subsequently adopt. Note that our value is older than the age estimated by Lachaume et al. (1999).

$\beta$  *Com*.—This is a G0 V star with a rotation period of about 12 days (Gray & Baliunas 1997). Its temperature and metal abundance (slightly supersolar) were determined by Barklem et al. (2002) and Gray et al. (2001) from spectroscopic analyses. Using the observed data, the evolutionary models of Girardi et al. (2000) yield a mass about 10% larger than the Sun and an age of  $2.3 \pm 1.1$  Gyr, in agreement with the remark of Gray & Baliunas (1997) about  $\beta$  *Com* being younger than the Sun. To refine the age estimate, we have used the rotation period–age relationship for solar-type stars of Guinan et al. (1998) and derived a value of  $\sim 1.6$  Gyr.

$\beta$  *Hyi*.—As pointed out by Dravins et al. (1998),  $\beta$  *Hyi*, of spectral type G2 IV, is our nearest subgiant star. A detailed study of  $\beta$  *Hyi* was published by Fernandes & Monteiro (2003), who also review determinations of stellar parameters, including the mass and age of  $\sim 6.7$  Gyr. We adopt the values in that recent work. The rotation period of  $\beta$  *Hyi* was determined from the analysis of 18 *IUE* High Dispersion LWP spectra obtained during 1994–1995 by E. F. G. under the SPREG program. Measurements of the chromospheric Mg II  $h$  and  $k$  emission-line fluxes relative to the adjacent continuum were made. The analysis reveals an apparent modulation in the relative Mg II  $h$  and  $k$  emission strength of  $P_{\text{rot}} = 29 \pm 3$  days, arising from chromospheric faculae and plages on the star (E. F. Guinan et al. 2005, in preparation).

There is an additional important issue yet to be addressed, the interstellar medium (ISM) column density along the targets' lines of sight. Although the stars in the sample are nearby and have negligibly small values of  $E(B - V)$  from ISM dust, some of the studied stellar emission features suffer strong ISM absorption and appropriate corrections need to be applied. The H I column densities in the lines of sight of our targets were estimated from the various lines of sight sampled by the H I Ly $\alpha$  observations of Wood et al. (2004). For  $\kappa^1$  *Cet* and  $\chi^1$  *Ori* direct measurements are available, whereas for the other four stars we employed the measured H I column densities for neighboring stars (selected on the basis of a similar distance and position). We used HD 116956 for EK Dra, DK UMa for  $\pi^1$  *UMa*, HZ 43 for  $\beta$  *Com*, and  $\zeta$  Dor,  $\epsilon$  Ind, and HD 203244 for  $\beta$  *Hyi*. The total adopted H I column densities in the target lines of sight are given in Table 1. These can be eventually scaled to compute the column densities of other elements from mean local ISM abundances.

### 3. OBSERVATIONAL DATA

Observations of the target stars in Table 1 were carried out with a variety of space-based instruments to maximize spectral coverage. Data from the following space missions have been used in the present study: the *Advanced Satellite for Cosmology and Astrophysics (ASCA)*, the *Röntgen Satellite (ROSAT)*, the *Extreme Ultraviolet Explorer (EUVE)*, the *Far Ultraviolet Spectroscopic Explorer (FUSE)*, the *Hubble Space Telescope (HST)*, and the *International Ultraviolet Explorer (IUE)*. As can be seen in the summary presented in Table 2, the observations discussed in this paper cover approximately the interval between 1 and 1700 Å, except for a gap between 360 and 920 Å, which is a region of very strong ISM absorption (H I Ly $\alpha$  continuum), thus far largely unexplored for stars other than the Sun. The number of data sets used for this study is quite extensive, and thus, all observation identification files for each target and mission are

TABLE 2  
SUMMARY OF SPACE MISSIONS USED IN THIS INVESTIGATION

Instrument	Wavelength range (Å)	Calibration Method
<i>ASCA</i> .....	1–40	Multi- $T_e$ plasma model
<i>ROSAT</i> .....	6–124	Multi- $T_e$ plasma model
<i>EUVE</i> .....	80–760 <sup>a</sup>	Flux calibrated
<i>FUSE</i> .....	920–1180	Flux calibrated
<i>HST</i> .....	1150–1730	Flux calibrated
<i>IUE</i> .....	1150–1950 <sup>b</sup>	Flux calibrated

<sup>a</sup> Wavelengths  $\lambda > 360$  Å are not useful because of strong interstellar absorption.

<sup>b</sup> With the SWP camera, for  $\lambda < 1700$  Å only.

TABLE 3  
OBSERVATION DATES AND IDS FOR ALL DATA SETS USED IN THIS INVESTIGATION

TARGET	DATE	OBS ID	DATE	OBS ID	DATE	OBS ID
	<i>ASCA</i>		<i>ROSAT</i> <sup>a</sup>		<i>EUVE</i>	
EK Dra.....	1994 May 24	22012000	1993 Oct 19	rp201474n00	1995 Dec 6	ek_dra__9512061129
$\pi^1$ UMa.....	1993 Nov 13	21018000	1993 Oct 5	rp201472n00	1998 Nov 30	3_uma__9811301325
	...	...	...	...	1998 Dec 5	3_uma__9812050029
$\chi^1$ Ori.....	...	...	...	...	1993 Jan 26	chi1_ori__9301261159
$\kappa^1$ Cet.....	1994 Aug 16	22013000	1993 Jul 27	rp201473n00	1994 Oct 13	kappa_cet__9410131500
	...	...	...	...	1995 Oct 6	kappa_cet__9510061036
$\beta$ Com.....	...	...	1993 Jun 17	rp201471n00	...	...
$\beta$ Hyi.....	...	...	1991 Apr 21	rp200071n00	...	...

TARGET	<i>FUSE</i>		<i>HST</i>		<i>IUE</i>	
EK Dra.....	2002 May 14	C1020501	...	...	1992 May 31	SWP 44817
$\pi^1$ UMa.....	2001 May 12	B0780101	...	...	1980 Mar 28	SWP 08582
	...	...	...	...	1990 Oct 12	SWP 39813
$\chi^1$ Ori.....	...	...	2000 Mar 10	o5bn02010	1990 Feb 1	SWP 38108
	...	...	2000 Mar 10	o5bn02020	1984 Apr 3	SWP 22408
$\kappa^1$ Cet.....	2000 Sep 10	A0830301	2000 Sep 19	o5bn03050	1994 Sep 14	SWP 52115
	...	...	2000 Sep 19	o5bn03060	1994 Aug 16	SWP 51829
	...	...	...	...	1994 Aug 16	SWP 51831
$\beta$ Com.....	2001 Jan 26	A0830401	...	...	1982 Feb 11	SWP 16313
	...	...	...	...	1979 Aug 14	SWP 06179
$\beta$ Hyi.....	2000 Jul 1	A0830101	...	...	1979 Dec 18	SWP 07430
	...	...	...	...	1979 Dec 3	SWP 07307
	...	...	...	...	1994 May 14	SWP 50765
	...	...	...	...	1992 Mar 13	SWP 44168

<sup>a</sup> EK Dra,  $\chi^1$  Ori,  $\kappa^1$  Cet, and  $\beta$  Hyi have *ROSAT* observations using the boron filter but were not used here.

listed in Table 3. All the observations described here, from both our guest observer programs and public data sets, were downloaded from the HEASARC<sup>5</sup> and MAST<sup>6</sup> archives.

### 3.1. X-Rays: *ASCA* and *ROSAT*

A key aspect of the study is the transformation of the instrumental fluxes into absolute fluxes, which is especially critical for the X-ray data. The observations obtained with *ASCA* and *ROSAT* are not naturally in absolute flux units and have to be compared with a physical plasma emission model to perform the calibration. The *ASCA* observations were obtained with the SIS0 and SIS1 detectors (Tanaka et al. 1994), and pointed observations with the PSPC (Briel & Pfeffermann 1995) were used with *ROSAT*. We reduced the X-ray data in the classical manner with the XSELECT, version 2.2, and XSPEC, version 11.3.0, packages within FTOOLS. Then, as is commonly done for coronal emissions (such as those from our solar analogs), we considered a multi- $T_e$  plasma and ran a  $\chi^2$  optimization fit with the MEKAL model (Mewe et al. 1995). In this procedure we followed exactly the same prescriptions as in Güdel et al. (1997b) and adopted plasma models with two and three components (obtaining results entirely consistent with this earlier study). Then, absolute fluxes were calculated from the best-fitting model with the aid of the XSPEC package. A correction for the H I column density using the values given in Table 1 was also included. A plot comparing the X-ray fluxes (*ASCA* and *ROSAT*) for the target stars is shown in Figure 1, where large differences (of up to a thousand-fold) become evident. Note that  $\chi^1$  Ori had only *ROSAT* observations taken with the boron filter (see footnote to Table 3). We decided not to use these here because of some calibration issues.

Güdel et al. (1997b), however, did analyze these data and obtained nearly the same parameters as those for  $\pi^1$  UMa (see their Tables 3 and 5), as expected from their similar ages.

### 3.2. EUV: *EUVE*

EUV observations of some of the targets were carried out as part of the *EUVE* mission (Malina & Bowyer 1991). In this

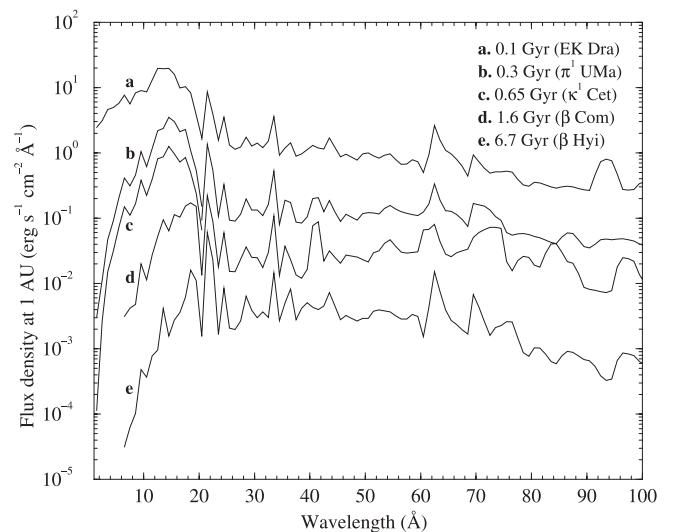


FIG. 1.—X-ray spectral irradiances (flux density at 1 AU vs. wavelength), covering different stages of the evolution of solar-type stars. The plot represents the fluxes in 1 Å bins as predicted by multi- $T$  plasma fits to *ASCA* and *ROSAT* observations (see text). Note the very large differences between young and old solar-type stars of up to a factor of 1000. [See the electronic edition of the *Journal for a color version of this figure.*]

<sup>5</sup> See <http://heasarc.gsfc.nasa.gov>.

<sup>6</sup> See <http://archive.stsci.edu>.

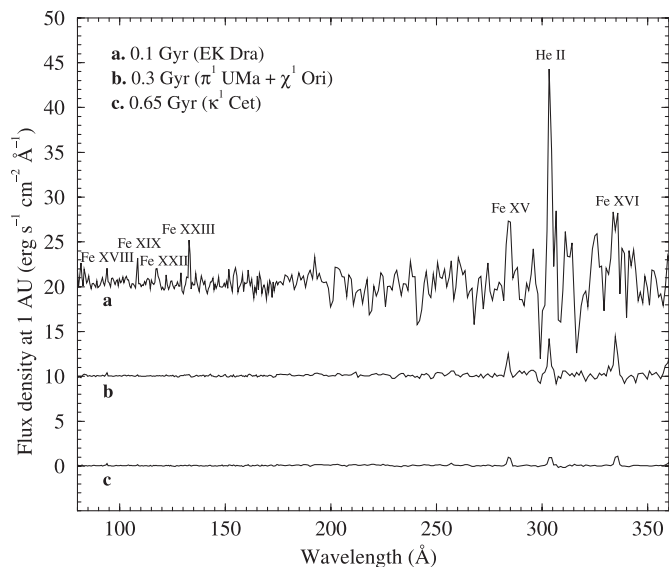


FIG. 2.—EUV irradiances (flux density at 1 AU vs. wavelength), covering different stages of the evolution of solar-type stars. Some relevant features are identified. The spectra have been zero point–shifted using integer multiples of  $10 \text{ ergs s}^{-1} \text{ cm}^{-2} \text{ \AA}^{-1}$  to avoid confusion. Note the decrease in emission-line strength from top to bottom (i.e., increasing age and rotation period). [See the electronic edition of the *Journal* for a color version of this figure.]

case, the resulting data can be directly flux-calibrated during reduction, and thus, no emission model has to be assumed beforehand. Data reduction of the *EUVE* spectra was carried out following the same procedure as in Güdel et al. (1997a). The only detail worth mentioning here is the correction of the H I column density, for which we assumed the values listed in Table 1. An illustration of the EUV fluxes for the observed targets is presented in Figure 2. The spectra of  $\pi^1$  UMa and  $\chi^1$  Ori, which correspond to the same stellar age, were averaged together. Note that most of the output stellar flux is associated with emission lines of highly ionized element transitions.

### 3.3. FUV: FUSE

To obtain irradiances in the FUV we carried out observations with *FUSE* using its large aperture (Moos et al. 2000). For a detailed description of the data sets used and the reduction procedure the reader is referred to Guinan et al. (2003), and thus, we skip that discussion here. The reductions in Guinan et al. also included the correction of ISM absorption in the emission features whenever necessary. To illustrate the irradiance differences among the observed targets, we show a detail of *FUSE* spectra in Figure 3. The complete *FUSE* spectra are not shown for the sake of clarity (see Guinan et al. 2003 for the identification of the strongest features), and the region illustrated is a wavelength window around two strong O VI emission lines. Again, a steep flux decrease with increasing age is evident.

### 3.4. UV: IUE and HST

UV spectroscopic observations of two of the stars in Table 1 ( $\chi^1$  Ori and  $\kappa^1$  Cet) were obtained with *HST* within program 8280. Thanks to the small aperture and the large spectral resolution used (STIS E140M echelle grating and  $0''.2 \times 0''.2$  aperture), these observations are ideally suited to study the strong H I Ly $\alpha$  emission line, besides other emission lines in the UV. The estimation of the integrated flux of the H I Ly $\alpha$  line requires careful correction for interstellar H I and D I absorption, which is significant even for the low column densities of our targets.

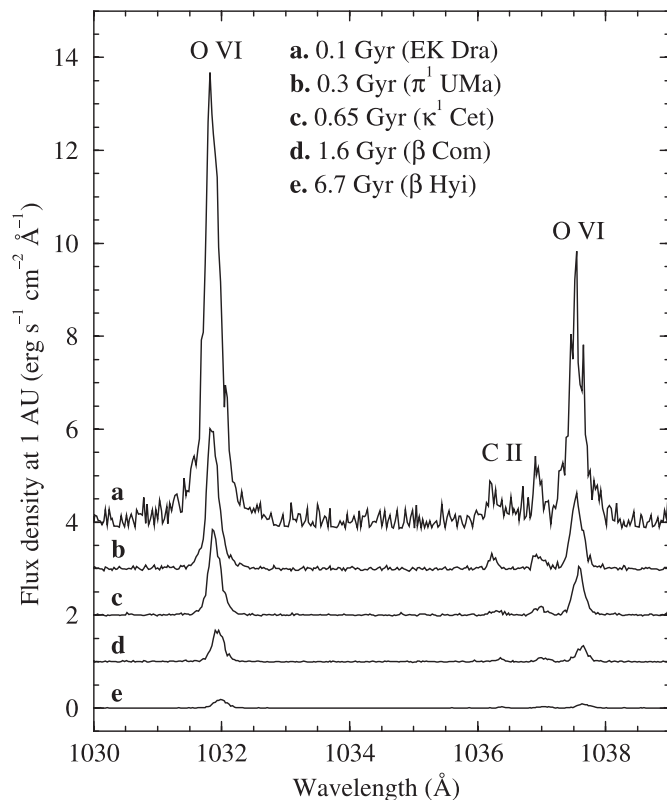


FIG. 3.—Details of the FUV irradiances for different stages of the evolution of solar-type stars in the region around the O VI  $\lambda\lambda 1032, 1038$  doublet. The spectra have been zero point–shifted using integer multiples of  $1 \text{ ergs s}^{-1} \text{ cm}^{-2} \text{ \AA}^{-1}$  to avoid confusion. Note the obvious trend of decreasing flux with increasing stellar age. [See the electronic edition of the *Journal* for a color version of this figure.]

Full details on this procedure and the data sets used can be found in Wood et al. (2004). A comparison of the H I Ly $\alpha$  emission features (with both the observed and rectified line profiles) for the two targets observed is shown in Figure 4.

The UV irradiances of the target stars up to  $1700 \text{ \AA}$  were completed with the *IUE* short-wavelength camera (SWP) low-dispersion observations (e.g., Kondo et al. 1989). Flux-calibrated data files are available from the MAST archive following the NEWSIPS calibration pipeline (Nichols & Linsky 1996). However, further correction to the fluxes was applied in accordance with the investigation of Massa & Fitzpatrick (2000). The bulk of the flux in the UV region shortward of  $1700 \text{ \AA}$  is in the form of emission lines, with a negligibly small photospheric continuum contribution. The comparison in Figure 5 depicts *IUE* spectra of the observed stars, in which the decrease of emission-line fluxes with age is apparent. The strongest features in the *IUE* range are labeled in Figure 5 and correspond to O I  $\lambda 1304$  (triplet), C II  $\lambda 1335$  (triplet),<sup>7</sup> Si IV  $\lambda 1400$  (doublet), C IV  $\lambda 1550$  (doublet), He II  $\lambda 1640$  (multiplet), and C I  $\lambda 1657$  (multiplet). As mentioned above an important issue for some of the emission lines is the correction of ISM absorption. Given the low electron density in the ISM (e.g., Spitzer & Fitzpatrick 1993; Wood & Linsky 1997), only transitions involving ground levels are expected to experience noticeable ISM absorption. All the emission features listed above except He II  $\lambda 1640$  have at least one ground-level transition component. For lines of Si IV, C IV, and C I, the very low abundance of

<sup>7</sup> One of the components is very weak and separated by only  $0.04 \text{ \AA}$  from a strong component.

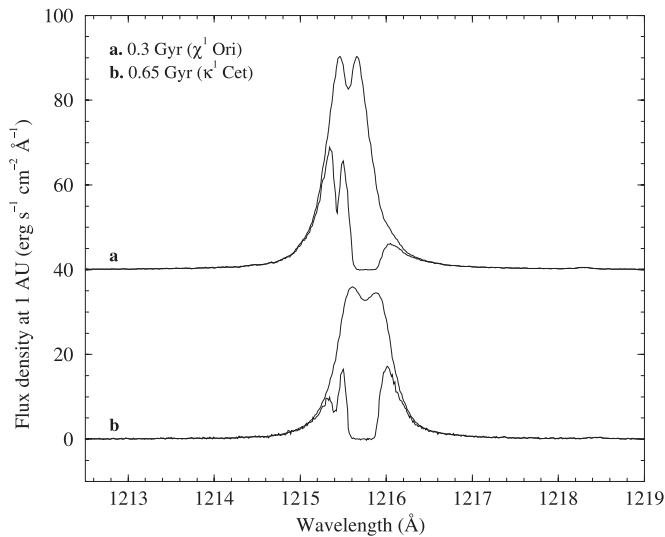


FIG. 4.—Detail of the H I Ly $\alpha$  line of two solar-type stars of different ages. The thin lines show the observed profiles from *HST* spectra, whereas the thick lines depict the reconstructed line profiles after correction for H I and D I ISM absorption. Irradiances are obtained by integrating the absorption-corrected profiles. The top spectrum has been shifted by  $40 \text{ ergs s}^{-1} \text{ cm}^{-2} \text{ \AA}^{-1}$  to avoid confusion. [See the electronic edition of the *Journal* for a color version of this figure.]

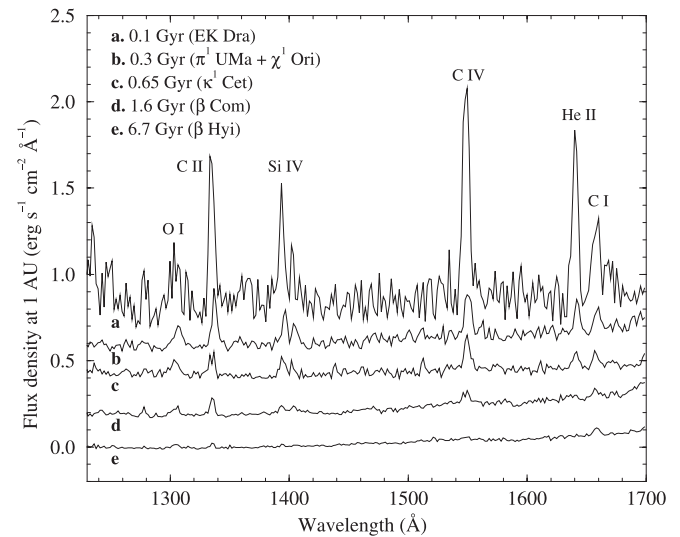


FIG. 5.—UV irradiances of solar-type stars at different stages of evolution. Some relevant features are identified. The emission-line strength is found to decrease from top to bottom (i.e., increasing age and rotation period). The spectra have been zero point–shifted using integer multiples of  $0.2 \text{ ergs s}^{-1} \text{ cm}^{-2} \text{ \AA}^{-1}$  to avoid confusion. When compared with the *EUVE* and *FUSE* spectra, the emission lines seem broader here because of the lower spectral resolution of the observations. Note the onset of some weak photospheric (continuum) flux above  $1500 \text{ \AA}$ . [See the electronic edition of the *Journal* for a color version of this figure.]

these species in the ISM (largely dominated by C II and Si II; see Wood et al. 2002b) implies negligible absorption along the lines of sight of our targets, rendering any correction unnecessary. For the triplets O I  $\lambda 1304$  and C II  $\lambda 1335$ , one of the components has a ground-state transition that is prone to ISM absorption, which we corrected as explained below.

To complement the *IUE* UV data, we used the *HST* echelle spectra described above for  $\chi^1$  Ori and  $\kappa^1$  Cet, which cover a wavelength interval from  $1150$  to  $1700 \text{ \AA}$ . These higher resolution data served the double purpose of cross-checking the integrated fluxes and carrying out a direct correction for ISM absorption. Inspection of the line profiles indicate that ISM absorption is present in the O I  $\lambda 1302.17$  and C II  $\lambda 1334.53$  components. These account for about 30% and 40% of the total flux of the O I and C II triplets, respectively. We carried out a reconstruction of the line profiles, assuming a Gaussian functional form with a superposed absorption (a total of six free parameters). For  $\kappa^1$  Cet, the difference in radial velocity between the star and the ISM components is only  $\sim 5 \text{ km s}^{-1}$ , thus implying significant absorption. In this case, the corrections to the total O I  $\lambda 1304$  and C II  $\lambda 1335$  fluxes were 14% and 20%, respectively. The resulting profile reconstruction parameters were found to agree very well with the ISM properties in the  $\kappa^1$  Cet line of sight (Wood et al. 2004). For  $\chi^1$  Ori, the radial velocity difference between the star and the absorbing ISM is  $\sim 36 \text{ km s}^{-1}$ , which makes the flux correction negligible ( $< 2\%$ ). Approximate corrections for the rest of the stars were computed from the results for  $\chi^1$  Ori and  $\kappa^1$  Cet and the properties of the ISM-absorbing components in Wood et al. (2004) by using the line-of-sight proxies discussed in § 2. The resulting corrections to the total O I  $\lambda 1304$  and C II  $\lambda 1335$  fluxes were in the range 2%–17%.

### 3.5. Solar Irradiance

Finally, we describe the mean solar irradiance spectrum used in our comparisons. As a consequence of an increasing number of sounding rocket experiments and space missions, knowledge

of the Sun’s high-energy emissions has improved considerably in recent times. In our investigation we used the detailed irradiances constructed by Woods et al. (1998 and references therein) from measurements made by sounding rockets and the UARS *SOLSTICE* mission. The data products available<sup>8</sup> include low-resolution ( $10 \text{ \AA}$ ) spectra and line-integrated fluxes for 1992, 1993, and 1994 and a high-resolution ( $1 \text{ \AA}$ ) spectrum for 1994. All these years correspond to solar cycle 22, with 1992 and 1993 representing moderate solar activity levels and 1994 representing the quiet Sun. We used data from 1993, which corresponds to midcycle, as representative of the Sun at the “average” activity level. The rocket and UARS *SOLSTICE* observations cover a wavelength interval from  $20$  to  $2000 \text{ \AA}$ . Because of the relatively low resolution of the observations ( $\sim 2 \text{ \AA}$ ), we used the higher resolution solar data from the SMM UVSP atlas<sup>9</sup> and the high-resolution spectrum of  $\alpha$  Cen A of Pagano et al. (2004) to check for possible contamination by blends in the interval  $\lambda > 1300 \text{ \AA}$ . Complementary soft X-ray irradiance measurements from the SNOE experiment (Bailey et al. 2000) were also used in the interval  $20$ – $200 \text{ \AA}$ . To complete the necessary short-wavelength data (hard X-rays), we used the inferred solar flux in the *ASCA* wavelength interval ( $1$ – $20 \text{ \AA}$ ) by Güdel et al. (1997b). The resulting energy distribution is in generally good agreement with the measurements made by the *GOES 10* and *12* satellites in the narrower  $1$ – $8 \text{ \AA}$  range.

## 4. MEASUREMENT AND ESTIMATION OF IRRADIANCES

One of the ultimate goals of the Sun in Time project is to produce a set of data products describing the high-energy irradiance evolution of the Sun and solar-type stars across the main sequence. These fluxes can then be used as input to model solar system planet and exoplanet atmospheres and study their

<sup>8</sup> See [http://lasp.colorado.edu/rocket/rocket\\_results.html](http://lasp.colorado.edu/rocket/rocket_results.html).

<sup>9</sup> See [ftp://umbra.nascom.nasa.gov/pub/uv\\_atlases](ftp://umbra.nascom.nasa.gov/pub/uv_atlases).

TABLE 4  
INTEGRATED FLUXES

$\lambda$ Interval (Å)	0.10 Gyr (EK Dra)	0.30 Gyr ( $\pi^1$ UMa+ $\chi^1$ Ori)	0.65 Gyr ( $\kappa^1$ Cet)	1.6 Gyr ( $\beta$ Com)	4.56 Gyr (Sun)	6.7 Gyr ( $\beta$ Hyi)
1–20 .....	180.2	21.5	7.76	0.976	0.15	0.048
20–100 .....	82.4	14.8	10.7	2.80	0.70	0.321
100–360 .....	187.2	69.4	22.7	(7.7)	2.05	(1.37)
360–920 .....	((45.6))	((15.2))	((7.0))	((2.85))	1.00	((0.68))
920–1180 .....	(18.1)	8.38	2.90	(1.70)	0.74	(0.50)
1–360 plus 920–1180 .....	467.9	114.1	44.1	13.2	3.64	2.2
1–1180 .....	513.5	129.3	51.1	16.0	4.64	2.9

NOTES.—Units of fluxes are  $\text{ergs s}^{-1} \text{cm}^{-2}$  and are normalized to a distance of 1 AU and to the radius of a  $1 M_{\odot}$  star. See § 4.1 regarding the single and double parentheses.

variations over time. To present the observational data described in § 3 we distinguish two separate components: integrated fluxes in wide wavelength intervals (roughly defined by the intervals covered by different missions) and emission fluxes of the strongest features in the high-energy spectrum. Data for six representative age stages are given: 100 Myr (EK Dra), 300 Myr ( $\pi^1$  UMa and  $\chi^1$  Ori), 650 Myr ( $\kappa^1$  Cet), 1.6 Gyr ( $\beta$  Com), 4.56 Gyr (Sun), and 6.7 Gyr ( $\beta$  Hyi). For 300 Myr, with two stellar proxies, we scaled the fluxes and computed averages whenever data for the two stars were available.

#### 4.1. Integrated Irradiances

The intervals considered are 1–20 Å (*ASCA*), 20–100 Å (*ROSAT*), 100–360 Å (*EUVE*), and 920–1180 Å (*FUSE*). Above 1180 Å we provide only the fluxes of the strongest features because of the difficulty in achieving a reliable total integration (caused by the increasing photospheric contribution). We will address this issue in a forthcoming publication. The total fluxes of the observed spectra were corrected to a distance of 1 AU and scaled (using a simple radius-squared relationship) to the expected radius of the Sun at the star’s age (in Table 1). The resulting stellar fluxes are presented in Table 4 (the values not in parentheses in the first five rows).

The measured fluxes show excellent correlations with the stellar ages (or, equivalently, with the rotation periods). The analysis reveals that the stellar fluxes can be very well approximated by power-law relationships, as illustrated in Figures 6a–6d. The parameters of the power-law fits are given in Table 5. Interestingly, the slopes of the best-fitting relationships decrease monotonically from the X-rays to the UV (i.e., decreasing energy or increasing wavelength). Thus, emissions associated with hotter plasmas diminish more rapidly, and the overall plasma cools down as the stars spin down with age. This behavior was already reported by earlier studies such as those by Ayres et al. (1981, 1999). Ayres (1997) gives also relationships for the relative flux variations at different wavelengths.

As noted above, the available observations are not complete because of two chief reasons. First, there is a gap between 360 and 920 Å for stars other than the Sun, and second, measurements could not be obtained for all targets in all wavelength intervals. The following targets have observations missing in some wavelength intervals: EK Dra (*FUSE*),  $\beta$  Com (*EUVE* and *FUSE*), and  $\beta$  Hyi (*EUVE* and *FUSE*). Note that in *FUSE* observations the lack of total flux values is caused by the impossibility of calculating the flux contribution from the H Lyman lines because of strong geocoronal contamination and saturated interstellar absorption (see Guinan et al. 2003 for further explanation). In the *EUVE* observations, two of the targets were

not observed because their predicted fluxes were below the detection limit of the instrument.

Having a (rough) estimate of the flux emitted by the stars in the intervals not covered by observations is rather critical, especially if the irradiances calculated in this work are to be used as input data in planetary atmosphere modeling. The estimation of fluxes for stars with no *FUSE* or *EUVE* observations is straightforward since the derived power laws can be employed to make predictions. Using this procedure, we calculated the predicted fluxes in Table 4 (the values in single parentheses in the first four rows) and a power-law fit to the integrated fluxes in the wavelength interval covered by the observations (Fig. 6e). With regard to the 360–920 Å interval, no expectations of having any observational data exist, even in the medium-term future. To circumvent this problem, there are at least three possible alternatives: (1) using empirical irradiances for the Sun with some ad hoc scalings to account for the various activity levels of our targets, (2) modeling from *EUVE* and UV by extrapolation under the assumption that the lines and the continuum are from the same plasma components, or (3) inferring the total integrated flux in the interval by comparison with the flux evolution in other wavelength ranges. We took the third approach chiefly because the accuracy we require is not very high (10%–20% is sufficient, as discussed below). In this way we avoid using solar data unsuitable for the very high activity level of some of our targets. In addition, the second method involves extrapolation from an incomplete range of plasma temperatures, since the observations cover only coronal temperatures ( $\sim$ MK) and the temperatures of a few FUV lines ( $\sim 10^5$  K). Given the power-law slopes in Table 5 for different wavelength regions, a value of  $-1.0$  seems to be a good compromise in the 360–920 Å interval. Thus, we calculated the flux predictions in Table 4 (the values in double parentheses) from the observed solar flux in this interval and the inferred power-law relationship. This crude interpolation could be flawed if strong emission lines were present in the wavelength interval. This does not seem to be the case when we inspect spectra from the Sun, such as the *SOLSTICE* data (see § 3.5), the *SOHO* SUMER spectral atlas (Curdt et al. 2001), or those from Procyon (Drake et al. 1995), but caution should be exercised when using the tabulated fluxes.

From the estimates described above, we were able to compute total irradiances in the interval 1–1180 Å, as given in the last row of Table 4. In addition, in Figure 6f we plot the total integrated fluxes and a power-law fit that yields an excellent fit to the data. An illustration of the spectral energy distribution of the targets is provided in Figure 7, in which the solid lines represent the observed data and the dashed lines have been calculated via power-law interpolation. In the complete wavelength

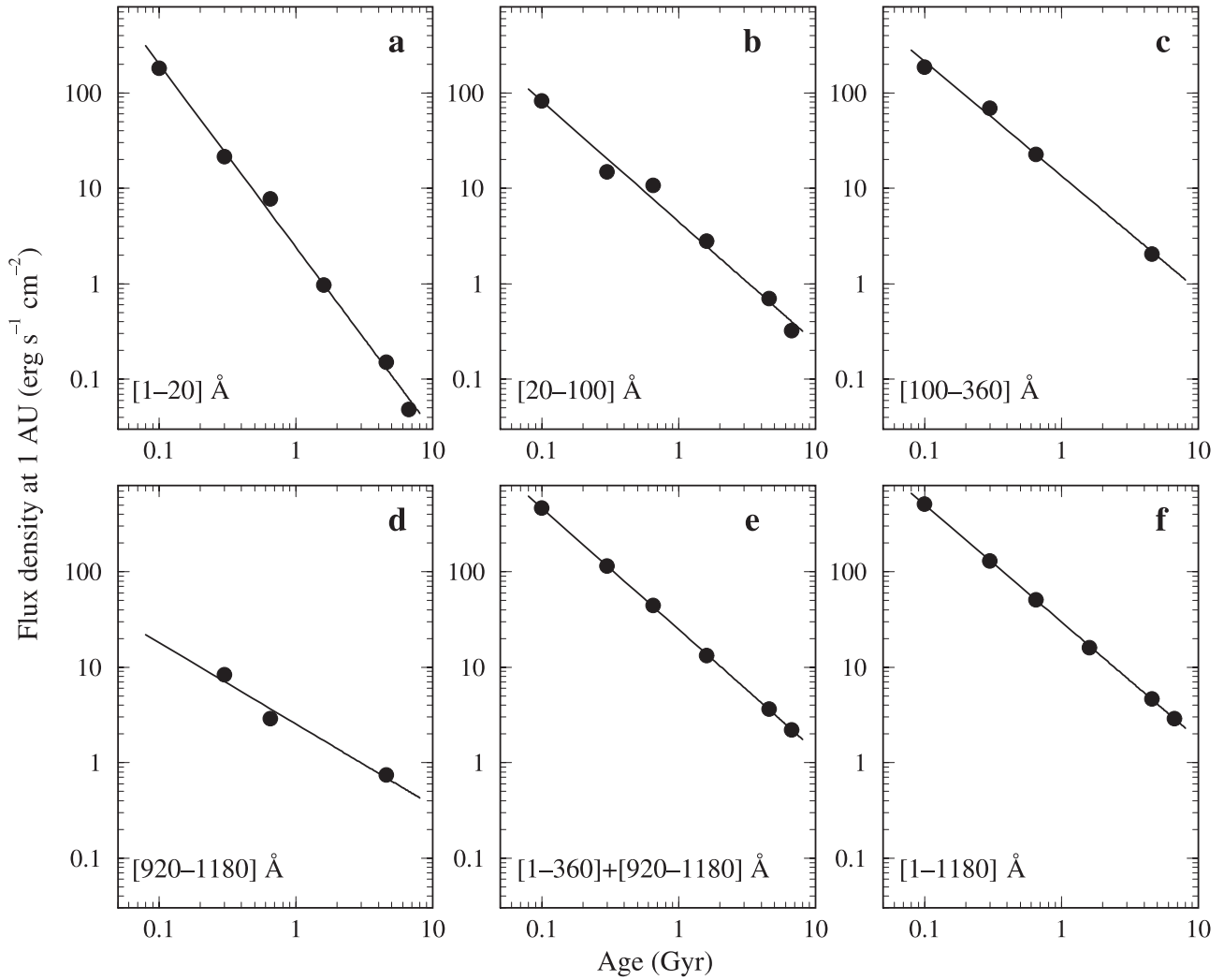


FIG. 6.—Power-law fits to the integrated irradiances in Table 4 for different wavelength intervals. The parameters of the resulting best-fitting relationships are given in Table 5.

interval, which is frequently used in aeronomy calculations, the flux ( $F$ ) as a function of stellar age ( $\tau$ ) is accurately reproduced by the expression (the upper wavelength limit can be extended from 1180 to 1200 Å because there are no additional relevant emission lines)

$$F = 29.7\tau^{-1.23} \text{ ergs s}^{-1} \text{ cm}^{-2}, \quad 1 \text{ \AA} < \lambda < 1200 \text{ \AA}, \quad (1)$$

TABLE 5  
PARAMETERS OF THE POWER-LAW FITS TO THE MEASURED INTEGRATED FLUXES

$\lambda$ Interval (Å)	$\alpha$	$\beta$
1–20.....	2.40	–1.92
20–100.....	4.45	–1.27
100–360.....	13.5	–1.20
360–920.....	4.56	(–1.0)
920–1180.....	2.53	–0.85
1–360 plus 920–1180.....	24.8	–1.27
1–1180.....	29.7	–1.23

NOTES.—Relationship of the form flux =  $\alpha\tau^\beta$ , where  $\alpha$  is a function of age in gigayears.

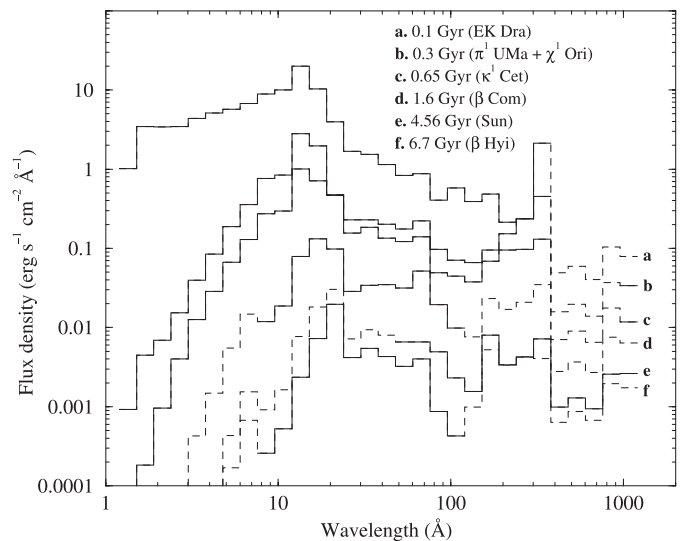


FIG. 7.—Full spectral energy distribution of the solar-type stars at different stages of the main-sequence evolution. The solid lines represent measured fluxes, whereas the dotted lines represent fluxes calculated by interpolation using a power-law relationship. [See the electronic edition of the Journal for a color version of this figure.]

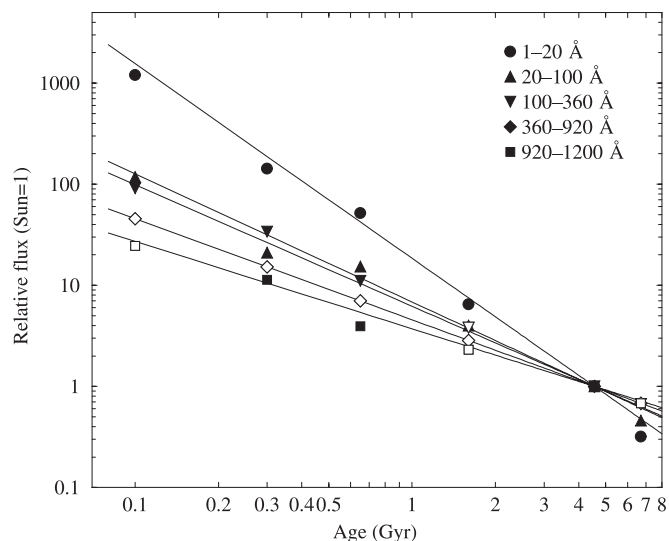


FIG. 8.—Solar-normalized fluxes vs. age for different stages of the evolution of solar-type stars. Plotted here are the measurements for different wavelength intervals (*filled symbols*) and the corresponding fits using power-law relationships with the slopes in Table 5. Represented with empty symbols are the inferred fluxes for those intervals with no available observations (the values in parentheses in Table 4).

where the stellar age  $\tau$  is in gigayears. Also illustrative is the plot in Figure 8, which represents the stellar fluxes normalized to the current solar values as a function of age. The steeper decrease of the higher energy emissions is evident in this plot. Also note that the emissions of the youngest stars in all wavelength intervals are orders of magnitude larger than the current solar flux.

#### 4.2. Line Fluxes

Line-integrated fluxes were measured for the strongest features of the high-energy spectrum whenever possible (i.e., with

sufficiently high instrumental resolution). As explained above, the observed fluxes were corrected for interstellar absorption (if necessary) and scaled to a distance of 1 AU and to the expected radius of the Sun at the star's age. The resulting line fluxes are presented in Table 6. Note that, as mentioned in § 3.5, the fluxes of the Sun for lines with  $\lambda > 1300 \text{ \AA}$  were checked for blends with high-resolution spectra. We found any contamination to be below a negligible 10%, and no further action was taken.

Similar to the total integrated fluxes, the line fluxes in Table 6 are also observed to follow well-defined power-law relationships as a function of stellar age, with the slopes given in Table 7. Also listed in this table are the characteristic ion formation temperatures, which can be regarded as the typical temperatures of the plasma where the line emissions originate (Arnaud & Rothenflug 1985). Similar to the integrated emissions, the flux decrease with age becomes more pronounced with higher formation temperatures (or, generally, shorter wavelengths).

Worth noting here is the powerful H I Ly $\alpha$  emission feature. As can be seen by comparing Tables 4 and 6, Ly $\alpha$  is a very significant contributor to the short-wave emission in the Sun and solar-type stars. This sole emission line produces a large fraction of the total flux between 1 and 1700 Å: from about 20% at 100 Myr up to over 50% for the current Sun. The observational data on Ly $\alpha$  irradiances of solar-type stars are still scarce, with only two targets measured thus far. The preliminary results presented here yield the following expression:

$$F = 19.2\tau^{-0.72} \text{ ergs s}^{-1} \text{ cm}^{-2}, \quad \text{H I Ly}\alpha. \quad (2)$$

Note that the formation temperature of this line is about 10 kK, so the power-law slope should be less steep but similar to that in the 920–1180 Å range, exactly as found (cf. Table 5). For comparison, the results of Wood et al. [2004; i.e.,  $F(\text{Ly}\alpha) \propto P_{\text{rot}}^{-(1.09 \pm 0.08)}$ ], when combined with the age–rotation period relationship of Ayres (1997; i.e.,  $P_{\text{rot}} \propto \tau^{-(0.6 \pm 0.1)}$ ), yield  $F(\text{Ly}\alpha) \propto \tau^{-(0.65 \pm 0.12)}$  for F and G dwarfs. It is worth noting that this

TABLE 6  
INTEGRATED FLUXES OF STRONG EMISSION FEATURES

$\lambda$ (Å)	Main Species	0.10 Gyr (EK Dra)	0.30 Gyr ( $\pi^1$ UMa+ $\chi^1$ Ori)	0.65 Gyr ( $\kappa^1$ Cet)	1.6 Gyr ( $\beta$ Com)	4.56 Gyr (Sun)	6.7 Gyr ( $\beta$ Hyi)
284.....	Fe xv	22.0	5.0	2.4	...	0.025	...
304.....	He II	44.3	8.3	2.3	...	0.260	...
335.....	Fe xvi	36.6	9.7	2.6	...	...	...
361.....	Fe xvi	15.7	6.6	1.6	...	0.016	...
584.....	He I	...	...	...	...	0.032	...
610, 625.....	Mg x	...	...	...	...	0.028	...
630.....	O v	...	...	...	...	0.037	...
789.....	O iv	...	...	...	...	0.017	...
834.....	O II	...	...	...	...	0.015	...
977.....	C III	5.0	1.22	0.59	0.30	0.150	0.124
1026.....	H I	...	3.1	0.80	...	0.098	...
1032.....	O vi	3.1	0.75	0.43	0.16	0.050	0.048
1038.....	O vi	1.5	0.38	0.21	0.074	0.025	0.022
1176.....	C III	3.4	0.73	0.37	0.15	0.053	0.046
1206.....	Si III	...	1.12	0.75	...	0.095	...
1216.....	H I	...	42.2	29.3	...	6.19	...
1304.....	O I	4.3	1.18	0.60	0.45	0.143	0.163
1335.....	C II	4.7	1.52	0.95	0.36	0.188	0.155
1400.....	Si IV	4.3	1.59	0.77	0.28	0.083	0.097
1550.....	C IV	9.1	2.21	1.02	0.40	0.146	0.082
1640.....	He II	6.0	0.99	0.56	...	0.040	...
1657.....	C I	4.1	0.97	0.78	0.47	0.202	0.210

NOTES.—Integrated units of fluxes are  $\text{ergs s}^{-1} \text{ cm}^{-2}$  and are normalized to a distance of 1 AU and to the radius of a  $1 M_{\odot}$  star. See text for details.

TABLE 7  
ION FORMATION TEMPERATURES AND SLOPES OF THE POWER-LAW  
FITS TO THE MEASURED LINE FLUXES IN TABLE 6

$\lambda$ (Å)	Main Species	$\log T$	Slope
284.....	Fe xv	6.30	-1.79
304.....	He ii	4.75	-1.34
335.....	Fe xvi	6.35	...
361.....	Fe xvi	6.35	-1.86
584.....	He i	4.25	...
610, 625.....	Mg x	6.08	...
630.....	O v	5.26	...
789.....	O iv	5.05	...
834.....	O ii	4.80	...
977.....	C iii	4.68	-0.85
1026.....	H i	3.84	-1.24
1032.....	O vi	5.42	-1.00
1038.....	O vi	5.42	-1.02
1176.....	C iii	4.68	-1.02
1206.....	Si iii	4.40	-0.94
1216.....	H i	3.84	-0.72
1304.....	O i	3.85	-0.78
1335.....	C ii	4.25	-0.78
1400.....	Si iv	4.75	-0.97
1550.....	C iv	5.00	-1.08
1640.....	He ii	4.75	-1.28
1657.....	C i	3.85	-0.68

slope is in remarkably good agreement with the value that we find.

Some studies have also revealed correlations between certain line fluxes and the overall high-energy flux. This is the finding of Bruner & McWhirter (1988), who reported a tight correlation between the C iv  $\lambda 1550$  flux and the total power radiated by solar active regions. We have carried out a similar comparison between the C iv  $\lambda 1550$  flux and the total integrated flux in the 1–1200 Å interval (cf. Table 7 and Fig. 8a of Bruner & McWhirter 1988). The power-law fit has a remarkable correlation coefficient of 0.998 and yields a slope of  $1.12 \pm 0.04$  (i.e.,  $F_{\text{tot}} \propto F_{\text{C iv}}^{1.12}$ ), in good agreement with the value 1.08 obtained by Bruner & McWhirter (the somewhat steeper slope in our case is likely due to excluding the UV flux, which would flatten the relationship). This argues strongly that the emissions of our targets arise from active regions that are similar to those of the Sun.

## 5. DISCUSSION

The comprehensive investigation presented here unequivocally demonstrates that the Sun has experienced a strong decrease of its high-energy emissions over the course of its main-sequence evolution. Quantitatively, the results indicate that the solar high-energy flux in the interval 1–1200 Å was about 2.5 times the present value 2.5 Gyr ago and about 6 times the present value about 3.5 Gyr ago. In addition, the 100 Myr ZAMS Sun should have had high-energy emissions some 100 times larger than those at present in this wavelength interval. The great diminishing of the solar high-energy flux with time is vividly illustrated by the following fact: the flux of EK Dra in the sole C iii  $\lambda 977$  emission line is larger than the entire integrated current solar irradiance below 1200 Å.

The results also show that an important contributor to the high-energy emissions of solar-type stars is the strong H i Ly $\alpha$  feature. This statement remains true throughout the lifetime of the stars, although the relative fraction of Ly $\alpha$  photons with

respect to the high-energy emissions increases with the age of the star. This investigation shows that the Ly $\alpha$  flux 2.5 and 3.5 Gyr ago was larger than today by factors of 1.8 and 2.9, respectively. Again, the 100 Myr old Sun was much more active, with an expected Ly $\alpha$  flux some 15 times larger than at present.

Note that the stellar sample we used covers the solar irradiance evolution from an age of about 100 Myr after its arrival on the main sequence. There are numerous indications that the Sun was even more active during the T Tauri and the early post-ZAMS stages (e.g., Simon et al. 1985 and references therein). Studies indicate that the X-ray luminosity of solar-type stars reaches a saturation level ( $\log L_X/L_{\text{bol}} \approx -3$ ) at a rotation period of about 1.5 days (Pizzolato et al. 2003). The X-ray emission of the youngest, most active solar-type stars can be up to 2–3 times higher than the flux of our youngest solar proxy, EK Dra. This is observed in stars of clusters such as  $\alpha$  Per or IC 2391, which have ages around 50 Myr. Analogous saturation effects are expected for the emissions in the EUV and UV ranges. The evolutionary stages younger than 100 Myr have strong significance for stellar evolution and dynamo theory, but also for the ionization of the accretion disk and hence, for planetary formation and astrochemistry. However, these early stages do not bear special relevance to studies related to planetary atmospheres and environments since planets were still forming in the protoplanetary nebula (Chambers & Wetherill 1998; Lissauer 1993). Even somewhat later in the evolution (up to  $\sim 500$  Myr), the influence of the strong solar irradiance may have been overwhelmed by the heavy bombardment period in the inner solar system (Sleep et al. 1989), as well as by planetary meltdowns and volcanism.

### 5.1. Previous Studies

Similar previous works on the same subject were published by Zahnle & Walker (1982) and Ayres (1997). The study of Zahnle & Walker (1982) focused on the evolution of solar ultraviolet emissions and was triggered by the early discoveries of high XUV luminosities of young late-type stars made by the *IUE* and *Einstein* satellites. The authors used T Tauri (pre-main sequence) stars and the current solar flux values to interpolate a flux evolution law for different wavelength intervals by assuming a  $t^{-1/2}$  scaling law for the rotational velocity. The results are in reasonable agreement with ours, in spite of the fact that Zahnle & Walker did not use a true solar analog sample and employed just two fiducial points for the interpolation. Ayres (1997) carried out a very detailed study of the solar high-energy flux, including a photoionization model for four species (H, O, O<sub>2</sub>, and N<sub>2</sub>), mostly focused on its application to the primitive Martian atmosphere. The author used a combination of empirical data (*EUVE*) and global scalings of the solar spectrum using power laws with slopes depending on the typical temperature formations of the ion species under study. In spite of the different approach, the results by Ayres are in generally good agreement with ours. Perhaps the power-law slopes reported by Ayres are slightly smaller, yet still compatible with those presented here.

### 5.2. Uncertainties, Cycles, and Variability

We have presented in § 4 the results of our XUV observations, but no error estimates have been discussed yet for the flux values. There are four chief sources of uncertainty in the stellar fluxes provided (if we neglect the errors associated with the radius and ISM absorption corrections): the measurement errors, the intrinsic variability of the emission, and the scatter

associated with the selection of the stellar proxies (i.e., we are assigning a single flux to a mass or spectral type interval). In turn, the error of the measurement has a contribution from the flux integration itself (photon noise) and from the calibration of the detector. The numerical error of the flux integration follows from the propagated error of the flux uncertainty in each wavelength bin.

We have carried out the necessary calculations and find that the observations were made with sufficiently long integration times that the photon noise contributes to an uncertainty of less than 5% on the measured fluxes. The exceptions to this are the integrated FUV fluxes, which have strong geocoronal contamination and had to be inferred by alternative methods (see Guinan et al. 2003), resulting in uncertainties of 20%–40%, and the *ROSAT* X-ray flux of  $\beta$  Hyi, with an uncertainty of about 10% due to the low count rate. The estimation of the calibration errors is quite often not straightforward. From the comparison between different X-ray missions and the absolute effective area calculations, one deduces an absolute calibration uncertainty on the order of 10%–20% for both *ASCA* SIS and *ROSAT* PSPC detectors.<sup>10</sup> For *EUVE*, Bowyer et al. (1996) report that the effective area calibration of each band is believed to be accurate to within 20%. For the *FUSE* LWRS LiF and SiC detectors, the absolute calibration of the fluxes has an uncertainty below 10%, according to the documentation on the *FUSE* Web site.<sup>11</sup> Detailed documentation is available on the absolute photometric accuracy of *HST* STIS MAMA echelle observations (as those used here), and the expected value is around 8%.<sup>12</sup> Finally, comparisons indicate that after correcting for systematic effects the absolute calibration of *IUE* is accurate to within 3% (Massa & Fitzpatrick 2000). Summarizing, we estimate that the measurement errors (including both photon noise and absolute calibration uncertainty) of the fluxes in Tables 4 and 6 decrease from about 10%–15% in the X-ray domain to about 5%–8% in the UV.

As mentioned above, there are additional sources of uncertainty caused by the intrinsic variability of the emission and by the differences between stars in the spectral range under study. Recall that the ultimate goal of this study is to obtain XUV fluxes for the Sun and solar-type stars over their (magnetic) evolutionary histories using stellar proxies. We are interested in obtaining the “average” XUV emissions that are characteristic of stars in a specific mass or spectral type window (G0–G5). With the available observations, there is very little we can say about the scatter caused by using stars that are slightly more massive than the Sun (see Table 1) as proxies. However, there are two competing effects that may cancel each other to a certain extent. On the one hand, more massive stars have larger surface areas and thus, larger integrated emissions, but, on the other hand, they also have shallower convective zones and a somewhat weaker dynamo. We may speculate that to first order the emissions of stars within a small interval of mass are very similar.

But certainly, the main contributor to the uncertainty of the fluxes in Tables 4 and 6 is caused by the intrinsic variability. It is well known that stellar magnetic activity is characterized by short- and medium-term variations over timescales of hours, days, months, and years. It is beyond the scope of this paper to analyze in detail the flux variations of all our solar proxies over

these timescales because that would imply a very large observational effort. In most cases, the available observations represent just a snapshot of the flux emissions without any reference to the “average” value and its scatter. We may, however, make an educated guess at the amplitude of the variations over timescales of years. In the Sun, besides flares, which are discussed below, the relevant source of midterm variability is the 11 yr activity cycle (see Lean 1997 for a complete review). In spite of the lack of accurate solar XUV variability measurements yet, the available data indicate solar maximum versus minimum (i.e., peak to peak) flux ratios of 10–20 for X-rays (10–100 Å), decreasing to ratios of about 2 at 600 Å and 1.2 at 1500 Å (Hinteregger 1981; Rottman 1988; Lean 1997). For the H I Ly $\alpha$  emission line, Woods et al. (2000) carried out a detailed study over different timescales and report a solar cycle peak-to-peak flux ratio of 1.5. The variability factor shows a positive correlation with the temperature of the associated emitting plasma. Thus, for specific lines the flux variations are a function of their formation temperatures (see Ayres 1997).

Solar-like stars have also been observed to exhibit activity cycles similar in length to that of the Sun (e.g., Baliunas & Vaughan 1985). For example, there is some yet inconclusive evidence for a 10–12 yr X-ray activity cycle in EK Dra (Güdel et al. 2003) and a cycle of similar length in  $\beta$  Hyi (E. F. Guinan 2004, unpublished). Interestingly, however, the flux maximum versus minimum ratio for EK Dra in the *ROSAT* band (i.e.,  $\approx$ 6–120 Å) is about 2.5, or some 4 times smaller than the Sun’s value (e.g., Hempelmann et al. 1996; Micela & Marino 2003). This may just be a consequence of the smaller contrast between maximum and minimum when the stars have high activity levels (i.e., surface active regions) at all times. An indication for possible long-term modulation depths can be obtained by observing cluster stars repeatedly, at intervals of several years. Such studies have been performed, for example, for the Pleiades cluster that contains many stars somewhat similar to EK Dra or for the Hyades, which are similar in age to  $\kappa^1$  Cet. These observing programs typically reported variations of no more than a factor of 2 for most stars; see, for example, Gagné et al. (1995), Micela et al. (1996), and Marino et al. (2003) for the Pleiades and Stern et al. (1994, 1995) for the Hyades.

The flux intrinsic variability with the activity cycle of our solar proxies will be the subject of a forthcoming study when the time baseline of the data permits a detailed investigation. At this point, taking into account all the available information, we estimate that total uncertainties for the power-law slopes in Table 5 are no larger than 0.1.

A further source of short-term variability is stellar flares. These are important for certain applications of our irradiance data because the amount of energy released in a single event can be significant. Observations of some of the solar proxies in our stellar sample indicate that flare events in young solar proxies such as EK Dra are frequent (about three or four major flares per day) and up to 100 times more powerful than those observed for the present Sun (Audard et al. 1999). X-ray flaring has also been observed on  $\pi^1$  UMa, and a large X-ray flare (10-fold X-ray enhancement) was recorded by the *EXOSAT* satellite during 1984 January (Landini et al. 1986). Another of our targets,  $\kappa^1$  Cet, experienced a flare that was recorded spectroscopically in the visible by Robinson & Bopp (1987). For an up-to-date study of X-ray flaring (which includes new observations of some of our targets), the reader is referred to the recent paper by Telleschi et al. (2005). In addition, we plan in the near future to use time-tagged spectra recently acquired with *FUSE* to address the evolution of the flare rates and energetics of solar-type stars

<sup>10</sup> See <http://heasarc.gsfc.nasa.gov>.

<sup>11</sup> See [http://fuse.pha.jhu.edu/analysis/calfuse\\_wp0.html](http://fuse.pha.jhu.edu/analysis/calfuse_wp0.html).

<sup>12</sup> See Space Telescope Imaging Spectrograph Instrument Handbook, <http://www.stsci.edu/hst/stis/documents> and Bohlin (1998).

over their lifetimes. We stress that the fluxes given in this paper are clear of major flare events and should constitute a faithful representation of the quiescent emission of the targets.

### 5.3. Particle Fluxes

With enhanced high-energy emissions and frequent flares, young solar-type stars are also expected to have more powerful particle winds. Evidence from the lunar and meteoritic fossil record agrees with this extrapolation and suggests that the Sun had a stronger wind in the past (e.g., Newkirk 1980). Similar conclusions were drawn by Lammer et al. (2000) from their study of the  $^{15}\text{N}/^{14}\text{N}$  isotope ratio in the atmosphere of Titan. The indirect evidence of an enhanced particle flux during the first 500 Myr of its life would be more compelling if a direct detection of the wind of a solar-type star was attained. Attempts made by Gaidos et al. (2000) to detect the winds of  $\pi^1$  UMa,  $\kappa^1$  Cet, and  $\beta$  Com from their radio emissions yielded null results. In addition, the search for blueshifted absorption in coronal lines carried out by Ayres et al. (2001) was unsuccessful.

Although winds of solar-like stars have not yet been detected directly, Wood et al. (2001, 2002a) devised a method to infer their characteristics from observations of the interaction between the fully ionized coronal winds and the partially ionized local ISM. Modeling of the associated absorption features, which are formed in the “astrospheres,” has provided the first empirical estimates of coronal mass-loss rates for G–K main-sequence stars. From the small sample for which the astrospheres can be observed, the mass-loss rates appear to increase with stellar activity. Using simple relationships involving rotational velocities and X-ray fluxes, Wood et al. (2002a) suggest that the mass-loss rate of the Sun has decreased, following a power law proportional to  $t^{-2}$ , which implies that the wind of the active young Sun may have been around 1000 times more massive than it is today. There are still a number of assumptions that have to be validated before this result can be fully established, especially the correlation between X-ray flux and mass-loss rate, as these originate from physically distinct regions (closed and open fields, respectively), but the work of Wood et al. is an important step forward.

With many of the solar wind characteristics still being unveiled today, it is not surprising that our knowledge of the particle fluxes of solar-type stars of different ages is at a very early stage. Evidence from independent sources indicates that the young Sun (and by extension, young solar-type stars) had a wind significantly more intense than at present. In addition, the high frequency of large flares observed with *EUVE* by Audard et al. (2000) in young suns such as EK Dra and 47 Cas B could indicate explosive episodic releases of plasma, generating non-thermal high-energy particles. These would be like the coronal mass ejections observed on the Sun but hundreds of times stronger and more frequent. Similar to those in the Sun today (Lewis & Simnett 2000; Schrijver & Zwann 2000), coronal mass ejections could contribute significantly to the stellar wind. As we discuss below, the solar wind plays an important role in the shaping and evolution of planetary atmospheres and surfaces and thus is an important component in characterizing the magnetic activity evolution of the Sun over its lifetime.

## 6. APPLICATIONS OF THE SOLAR IRRADIANCE DATA

### 6.1. Thermal Escape on Exoplanets

The high-energy irradiance evolution data presented in this paper are intended to be an ingredient of studies related to the evolution of solar system planets and exoplanets. Meier (1991)

gives the absorption profile of the Earth’s atmosphere and shows that most of the radiation with  $\lambda \lesssim 1700 \text{ \AA}$  is absorbed (and thus deposits its energy) in the thermosphere, at an altitude above 90 km. Similar effects are found in atmospheres with different compositions (e.g., within the solar system) since the absorption cross sections of the high-energy photons of all the atomic species present in the upper atmospheres are very large. Thus, XUV ionizing radiation raises the temperature of the planetary thermospheres and affects their vertical temperature profiles and energy transport mechanisms. Obviously, planets around young solar-type stars, with XUV fluxes 10–100 times stronger than those of today’s Sun, suffer intense heating of their upper atmospheres, which reaches temperatures much above the current value of 1000 K for the Earth. When the temperature of the thermosphere is large, a significant fraction of the light constituents of the upper atmosphere attain velocities above the escape value (and drag heavier constituents away).

Thermal escape, although commonly neglected in studies of the present solar system, may be important in planets around magnetically active stars. Thus, any attempt to calculate the history of a planet’s atmosphere around a solar-type star needs to include the XUV energy evolution, since this regulates the efficiency of evaporation processes. Calculations using early data from the present work were carried out by Lammer et al. (2003b), who showed that “hot Jupiters” could lose significant fractions of their hydrogen masses under intense XUV radiation. Non-thermal mechanisms caused by ionosphere–stellar wind interactions also contribute to this loss process (Grießmeier et al. 2004). The tantalizing results indicate that hydrogen-rich giant exoplanets may suffer rapid evaporation under strong XUV radiation conditions. Once the entire hydrogen envelope is lost, only the rocky planetary cores would remain, thus representing a putative new class of planet. The confirmation of the theoretical prediction of thermal escape comes from the observations of Vidal-Madjar et al. (2003), who reported a large exospheric radius for the transiting planet HD 209458b (due to thermal expansion) and a loss rate compatible with the estimates of Lammer et al. The consequences of this enhanced thermal loss process could explain the apparent paucity of exoplanets so far detected at very close orbital distances ( $<0.05 \text{ AU}$ ). Terrestrial planets could also be affected by the enhanced XUV environment and lose a significant fraction of their lighter atmospheric constituents.

### 6.2. The Martian Water Inventory

The Sun in Time data are also being used to study aspects related to the evolution of solar system planet atmospheres and surfaces. In particular, the planet Mars has been especially vulnerable in the past to the influence of the Sun’s energy and particle emissions because of its small mass and lack of a protecting magnetic field. Lammer et al. (2003a) and Terada et al. (2005) have studied the Martian water inventory using reliable solar XUV and wind evolution laws and comprehensive models for the loss processes of hydrogen and oxygen that include dissociative recombination, ion pickup, sputtering, and viscous processes in the planet’s ionosphere. The more recent work of Terada et al. uses a global hybrid model to conclude that the loss of  $\text{H}_2\text{O}$  from Mars over the last 3.5 Gyr is equivalent to a global Martian ocean with a depth of about 10.5 m. This value is smaller than those reported by previous studies but could still be slightly overestimated.

The two studies quoted also find that the sum of thermal and nonthermal atmospheric loss rates of H and all nonthermal escape processes of O to space are not compatible with a ratio of 2:1 (H to O) expected from the atomic composition of water

and are currently close to about 20 : 1. Escape to space cannot therefore be the only sink for oxygen on Mars. These results suggest that the missing oxygen can be explained by its incorporation into the Martian surface by chemical weathering processes since the onset of intense oxidation about 2 Gyr ago. This oxygen incorporation also has implications for the oxidant extinction depth, which is an important parameter in determining the sampling depths required for searching for organic material on Mars. The oxidant extinction depth is expected to lie in a range between 2 and 5 m for global mean values.

### 6.3. Erosion of Mercury's Surface

The planet Mercury, because of its closeness to the Sun, suffered major exposure to particle and XUV emissions during its early active stages (see Guinan & Ribas 2004). Mercury's core is large compared with those of other terrestrial planets, extending out to over 60% of its radius. One of several hypotheses advanced to explain this anomaly is that strong dense winds and very high XUV fluxes of the young Sun (during the first 0.5–1 Gyr of its life) swept away its early atmosphere and much of its outer mantle. Even today (with a much less active Sun) ground-based observations of heavy constituents such as Na<sup>+</sup>, K<sup>+</sup>, and O<sup>+</sup> in Mercury's present transient exosphere implicate a strong exosphere-surface interaction related to the particle and radiation environment of the nearby Sun (e.g., Cameron 1985). Tehrany et al. (2002) have carried out initial calculations indicating that enhanced solar wind and XUV emissions could be sufficient to explain the present relatively thin mantle and relatively large iron core. If this hypothesis is correct, young Mercury may have started out similar in size to the Earth but lost much of its less dense mantle from radiation and particle interactions (ion pickup) with the young Sun.

### 6.4. The Paleoclimate of the Earth

Finally, the young Sun's emissions may have also had an impact on the early evolution of Earth's atmosphere. Besides heating the thermosphere and altering the vertical temperature profile, the enhanced high-energy flux can strongly influence the photochemistry and photoionization of the early planetary atmospheres and may play a role in the origin and development of life on Earth, as well as possibly on Mars. For example, Canuto et al. (1982, 1983) discuss the photochemistry of O<sub>2</sub>, O<sub>3</sub>, CO<sub>2</sub>, H<sub>2</sub>O, etc., in the presumed CO<sub>2</sub>-rich early atmosphere of the Earth. In this context, the Ly $\alpha$  flux plays an important role, as it is strong enough to penetrate the planetary exospheres into their mesospheres, richer in molecules, and susceptible to photochemical reactions.

The Sun in Time data can also provide insights into the so-called Faint Sun Paradox (see Guinan & Ribas 2002). The paradox arises from the fact that standard stellar evolutionary models show that the ZAMS Sun had a bolometric luminosity of ~70% of the present Sun. This should have led to a much cooler Earth in the past, whereas geological and fossil evidence indicates otherwise. A solution to the Faint Sun paradox proposed by Sagan & Mullen (1972) was an increased greenhouse effect on the early Earth. The gases that have been suggested to account for this enhanced greenhouse effect are CO<sub>2</sub>, NH<sub>3</sub>, or CH<sub>4</sub> (see, e.g., Rye et al. 1995; Sagan & Chyba 1997; Pavlov et al. 2000). Although the stronger XUV solar radiation cannot by itself explain the Faint Sun Paradox (because it accounts for only an insignificant percentage of the Sun's radiative output), the photoionization and photodissociation reactions triggered could play a major role in which greenhouse gases are available. For example, the enhanced photodissociating FUV-UV radiation

levels of the young Sun may have influenced the abundances of ammonia and methane in the prebiotic and Archean planetary atmosphere some 2–4 Gyr ago. Similarly, the photochemistry and abundance of O<sub>3</sub> is of great importance to the study of the genesis of life on Earth.

In summary, any model of the paleoatmosphere of the Earth and other solar system planets needs to account for the stronger XUV and particle radiation from the young Sun. If the XUV fluxes of the young Sun are estimated by a simple scaling of the current values by a factor of 0.7 (in accord with the lower expected photospheric flux), this would represent a severe underestimation of the radiation levels by orders of magnitude.

## 7. CONCLUSIONS

One of the primary goals of the Sun in Time program is to reconstruct the spectral irradiance evolution of the Sun and, by extension, of solar-type stars. To this end, a large number of multiwavelength (X-ray, EUV, FUV, UV, and visible) observations have been collected and analyzed. The observations, secured with *ASCA*, *ROSAT*, *EUVE*, *FUSE*, *HST*, and *IUE*, cover 1 Å (12 keV) to 1700 Å, except for a gap between 360 and 920 Å, which is a region of very strong ISM absorption. Irradiance data are already available for five of the stars in our sample.

A detailed quantitative analysis reveals that the stellar fluxes can be very well approximated by power-law relationships. Interestingly, the slopes of the best-fitting relationships are seen to decrease monotonically from the X-ray to the UV band (i.e., decreasing energy or increasing wavelength). Emissions associated with hotter plasmas diminish more rapidly, and the overall plasma cools down as the stars spin down with age. The results from the Sun in Time program suggest that the coronal X-ray–EUV emissions of the young main-sequence Sun were ~100–1000 times stronger than those of the present Sun. Similarly, the transition region and chromospheric FUV-UV emissions of the young Sun are expected to be 20–60 and 10–20 times stronger, respectively, than presently. In the entire XUV interval from 1 to 1200 Å, we find that 2.5 Gyr ago the solar high-energy flux was about 2.5 times the present value and about 3.5 Gyr ago was about 6 times the present value (when life arose on Earth). In addition, preliminary estimates using spectra of two solar proxies indicate that Ly $\alpha$  flux of the young Sun was also much stronger, by up to a factor of 15. In addition to intense levels of dynamo-generated coronal and chromospheric XUV emissions, the young Sun and young solar analogs are also expected to have stronger and more frequent flares and to have stronger (more massive) stellar winds.

In summary, compelling observational evidence indicates that in the past the Sun underwent a much more active phase. The enhanced activity revealed itself in the form of strong high-energy emissions, frequent flares, and a powerful stellar wind. Such energy and particle environment certainly had an impact on the genesis and evolution of solar system planets and planetary atmospheres.

Besides completing remaining gaps in the data (e.g., Ly $\alpha$  irradiances, somewhat complicated by the demise of the STIS spectrograph on *HST*) and better characterizing the flare statistics and wind properties, future work will take two main directions. We plan to extend our study to longer wavelengths, between 1700 and 3000 Å. Here the photospheric emissions begin to dominate over those of the chromosphere and a lot more care has to be taken in adequately normalizing the flux, also because the emission differences between young and old solar-type stars are expected to be smaller (~10%–30%). The UV portion of the spectrum (UVA, UVB, and UVC) is of great

importance, as it drives the majority of the photochemical reactions and may influence the generation and destruction of some chemical compounds, e.g.,  $\text{NO}_x$ , that are important to life.

Because lower mass stars are especially common and hence may host habitable planets, progress in this direction has started by expanding the Sun in Time program to time sequences of the high-energy emissions, wind, and flare activity of low-mass K and M stars. These stars are far more numerous than the solar-type stars, have long main-sequence lifetimes, and, in principle, are prime targets for terrestrial planet searches. Because of the low luminosities, their “habitable zones” (see Kasting et al. 1993) can be quite close to the host stars. Low-mass stars have deeper outer convective zones (where the magnetic dynamo operates) than Sun-like stars and thus possess very efficient magnetic dynamos. The expected enhanced XUV radiation environment should play a major role in the development of the atmospheres and ultimately of life on planets located in their habitable zones.

## REFERENCES

- Arnaud, M., & Rothenflug, R. 1985, *A&AS*, 60, 425
- Audard, M., Güdel, M., Drake, J. J., & Kashyap, V. L. 2000, *ApJ*, 541, 396
- Audard, M., Güdel, M., & Guinan, E. F. 1999, *ApJ*, 513, L53
- Ayres, T. R. 1997, *J. Geophys. Res.*, 102(E1), 1641
- . 1999, *ApJ*, 525, 240
- Ayres, T. R., Brown, A., Osten, R. A., Huenemoerder, D. P., Drake, J. J., Brickhouse, N. S., & Linsky, J. L. 2001, *ApJ*, 549, 554
- Ayres, T. R., Marstad, N. C., & Linsky, J. L. 1981, *ApJ*, 247, 545
- Bailey, S. M., Woods, T. N., Barth, C. A., Solomon, S. C., Canfield, L. R., & Korde, R. 2000, *J. Geophys. Res.*, 105(A12), 27179
- Baliunas, S. L., & Vaughan, A. H. 1985, *ARA&A*, 23, 379
- Barklem, P. S., Stempels, H. C., Allende Prieto, C., Kochukhov, O. P., Piskunov, N., & O’Mara, B. J. 2002, *A&A*, 385, 951
- Barrado y Navascués, D., Stauffer, J. R., & Randich, S. 1998, *ApJ*, 506, 347
- Bohlin, R. 1998, STIS Instrument Science Report 98-18, <http://www.stsci.edu/hst/stis/documents/isrs>
- Bowyer, S., Lampton, M., Lewis, J., Wu, X., Jelinsky, P., & Malina, R. F. 1996, *ApJS*, 102, 129
- Briel, U. G., & Pfeiffermann, E. 1995, *Proc. SPIE*, 2518, 120
- Bruner, M. E., & McWhirter, R. W. P. 1988, *ApJ*, 326, 1002
- Cameron, A. G. W. 1985, *Icarus*, 64, 285
- Canuto, V. M., Levine, J. S., Augustsson, T. R., & Imhoff, C. L. 1982, *Nature*, 296, 816
- Canuto, V. M., Levine, J. S., Augustsson, T. R., Imhoff, C. L., & Giampapa, M. S. 1983, *Nature*, 305, 281
- Chambers, J. E., & Wetherill, G. W. 1998, *Icarus*, 136, 304
- Cockell, C. S., Catling, D. C., Davis, W. L., Snook, K., Kepner, R. L., Lee, P., & McKay, C. P. 2000, *Icarus*, 146, 343
- Curd, W., Brekke, P., Feldman, U., Wilhelm, K., Dwivedi, B. N., Schühle, U., & Lemaire, P. 2001, *A&A*, 375, 591
- Dorren, J. D., & Guinan, E. F. 1994, in *IAU Coll. 143, The Sun as a Variable Star*, ed. J. M. Pap, C. Frölich, H. S. Hudson, & S. K. Solanki (Cambridge: Cambridge Univ. Press), 206
- Drake, J. J., Laming, J. M., & Widing, K. G. 1995, *ApJ*, 443, 393
- Dravins, D., Lindgren, L., & Vandenberg, D. A. 1998, *A&A*, 330, 1077
- Duquennoy, A., & Mayor, M. 1991, *A&A*, 248, 485
- Durney, B. 1972, in *Solar Wind*, ed. C. P. Sonett, P. J. Coleman, & J. M. Wilcox (Washington: NASA), 282
- Fernandes, J., & Monteiro, M. J. P. F. G. 2003, *A&A*, 399, 243
- Gagné, M., Caillault, J.-P., & Stauffer, J. R. 1995, *ApJ*, 450, 217
- Gaidos, E. J., & González, G. 2002, *NewA*, 7, 211
- Gaidos, E. J., Güdel, M., & Blake, G. A. 2000, *Geophys. Res. Lett.*, 27, 501
- Girardi, L., Bressan, A., Bertelli, G., & Chiosi, C. 2000, *A&AS*, 141, 371
- Gratton, R. G., Carretta, E., & Castellì, F. 1996, *A&A*, 314, 191
- Gray, D. F., & Baliunas, S. L. 1997, *ApJ*, 475, 303
- Gray, R. O., Graham, P. W., & Hoyt, S. R. 2001, *AJ*, 121, 2159
- Griebmeier, J.-M., et al. 2004, *A&A*, 425, 753
- Güdel, M., Guinan, E. F., Mewe, R., Kaastra, J. S., & Skinner, S. L. 1997a, *ApJ*, 479, 416
- Güdel, M., Guinan, E. F., & Skinner, S. L. 1997b, *ApJ*, 483, 947
- Güdel, M., et al. 2003, in *The Future of Cool-Star Astrophysics: 12th Cambridge Workshop on Cool Stars, Stellar Systems, and the Sun*, ed. A. Brown, G. M. Harper, & T. R. Ayres (Boulder: Univ. of Colorado), 303
- Guinan, E. F., Güdel, M., & DeWarf, L. E. 1998, in *Solar Analogs: Characteristics and Optimum Candidates*, ed. J. C. Hall (Flagstaff: Lowell Obs.), 61
- Guinan, E. F., & Ribas, I. 2002, in *ASP Conf. Ser. 269, The Evolving Sun and its Influence on Planetary Environments*, ed. B. Montesinos, A. Giménez, & E. F. Guinan (San Francisco: ASP), 85
- . 2004, in *IAU Symp. 219, Stars as Suns: Activity, Evolution, and Planets*, ed. A. K. Dupree & A. O. Benz (San Francisco: ASP), 423
- Guinan, E. F., Ribas, I., & Harper, G. M. 2003, *ApJ*, 594, 561
- Hamilton, R. T., Guinan, E. F., & DeWarf, L. E. 2003, *BAAS*, 203, 4801
- Han, I., & Gatewood, G. 2002, *PASP*, 114, 224
- Hempelmann, A., Schmitt, J. H. M. M., & Stepien, K. 1996, *A&A*, 305, 284
- Hinteregger, H. E. 1981, *Adv. Space Res.*, 1, 39
- Kasting, J. F., & Catling, D. 2003, *ARA&A*, 41, 429
- Kasting, J. F., Whitmire, D. P., & Reynolds, R. T. 1993, *Icarus*, 101, 108
- King, J. R., Villarreal, A. R., Soderblom, D. R., Gulliver, A. F., & Adelman, S. J. 2003, *AJ*, 125, 1980
- Kondo, Y., Boggess, A., & Maran, S. P. 1989, *ARA&A*, 27, 397
- König, B., Fuhrmann, K., Neuhäuser, R., Charbonneau, D., & Jayawardhana, R. 2002, *A&A*, 394, L43
- Lachaume, R., Dominik, C., Lanz, T., & Habing, H. J. 1999, *A&A*, 348, 897
- Lammer, H., Lichtenegger, H., Kolb, C., Ribas, I., Guinan, E. F., & Bauer, S. J. 2003a, *Icarus*, 165, 9
- Lammer, H., Selsis, F., Ribas, I., Guinan, E. F., Bauer, S. J., & Weiss, W. W. 2003b, *ApJ*, 598, L121
- Lammer, H., Stumptner, W., Molina-Cuberos, G. J., Bauer, S. J., & Owen, T. 2000, *Planet. Space Sci.*, 48, 529
- Landini, M., Monsignori Fossi, B. C., Pallavicini, R., & Piro, L. 1986, *A&A*, 157, 217
- Lean, J. 1997, *ARA&A*, 35, 33
- Lewis, D. J., & Simnett, G. M. 2000, *Sol. Phys.*, 191, 185
- Lissauer, J. J. 1993, *ARA&A*, 31, 129
- Malina, R. F., & Bowyer, S. 1991, *Extreme Ultraviolet Astronomy* (New York: Pergamon)
- Marino, A., Micela, G., Peres, G., & Sciortino, S. 2003, *A&A*, 406, 629
- Massa, D., & Fitzpatrick, E. L. 2000, *ApJS*, 126, 517
- Meier, R. R. 1991, *Space Sci. Rev.*, 58, 1
- Messina, S., & Guinan, E. F. 2003, *A&A*, 409, 1017
- Messina, S., Rodonò, M., & Guinan, E. F. 2001, *A&A*, 366, 215
- Metchev, S. A., & Hillenbrand, L. A. 2004, *ApJ*, 617, 1330
- Mewe, R., Kaastra, J. S., & Liedahl, D. A. 1995, *Legacy*, 6, 16
- Micela, G., & Marino, A. 2003, *A&A*, 404, 637
- Micela, G., Sciortino, S., Kashyap, V., Hardten, F. R., Jr., & Rosner, R. 1996, *ApJS*, 102, 75
- Montes, D., López-Santiago, J., Fernández-Figueroa, M. J., & Gálvez, M. C. 2001a, *A&A*, 379, 976
- Montes, D., López-Santiago, J., Gálvez, M. C., Fernández-Figueroa, M. J., De Castro, E., & Cornide, M. 2001b, *MNRAS*, 328, 45
- Moos, H. W., et al. 2000, *ApJ*, 538, L1
- Newkirk, G., Jr. 1980, in *The Ancient Sun: Fossil Record in the Earth, Moon, and Meteorites*, ed. R. O. Pepin, J. A. Eddy, & R. B. Merrill (New York: Pergamon), 293
- Nichols, J. S., & Linsky, J. L. 1996, *AJ*, 111, 517
- Ottmann, R., Pfeiffer, M. J., & Gehren, T. 1998, *A&A*, 338, 661

- Pagano, I., Linksy, J. L., Valenti, J., & Duncan, D. K. 2004, *A&A*, 415, 331
- Parker, E. N. 1970, *ARA&A*, 8, 1
- Pavlov, A. A., Kasting, J. F., Brown, L. L., Rages, K. A., & Freedman, R. 2000, *J. Geophys. Res.*, 105(E5), 11981
- Pizzolato, N., Maggio, A., Micela, G., Sciortino, S., & Ventura, P. 2003, *A&A*, 397, 147
- Porto de Mello, G. F., & da Silva, L. 1997, *ApJ*, 482, L89
- Radick, R. R., Lockwood, G. W., Skiff, B. A., & Thompson, D. T. 1995, *ApJ*, 452, 332
- Robinson, C. R., & Bopp, B. W. 1987, in *Cool Stars, Stellar Systems, and the Sun*, Proc. 5th Cambridge Workshop, ed. J. L. Linsky & R. E. Stencel (Lecture Notes in Physics 291; Berlin: Springer), 509
- Rottman, G. J. 1988, in *Solar Radiative Output Variation*, ed. P. Foukal (Boulder: Natl. Cent. Atmos. Res.), 71
- Rye, R., Kuo, P. H., & Holland, H. D. 1995, *Nature*, 378, 603
- Sagan, C., & Chyba, C. 1997, *Science*, 276, 1217
- Sagan, C., & Mullen, G. 1972, *Science*, 177, 52
- Schrijver, C. J., & Zwann, C. 2000, *Solar and Stellar Magnetic Activity* (Cambridge: Cambridge Univ. Press)
- Simon, T., Boesgaard, A. M., & Herbig, G. 1985, *ApJ*, 293, 551
- Skumanich, A. 1972, *ApJ*, 171, 565
- Sleep, N. H., Zahnle, K. J., Kasting, J. F., & Morowitz, H. J. 1989, *Nature*, 342, 139
- Smith, D. S., Scalo, J., & Wheeler, J. C. 2004, *Icarus*, 171, 229
- Soderblom, D. R. 1982, *ApJ*, 263, 239
- Soderblom, D. R., & Mayor, M. 1993, *AJ*, 105, 226
- Spitzer, L., Jr., & Fitzpatrick, E. L. 1993, *ApJ*, 409, 299
- Stern, R. A., Schmitt, J. H. M. M., & Kahabka, P. T. 1995, *ApJ*, 448, 683
- Stern, R. A., Schmitt, J. H. M. M., Pye, J. P., Hodgkin, S. T., Stauffer, J. R., & Simon, T. 1994, *ApJ*, 427, 808
- Strassmeier, K. G., & Rice, J. B. 1998, *A&A*, 330, 685
- Tanaka, Y., Inoue, H., & Holt, S. S. 1994, *PASJ*, 46, L37
- Taylor, B. J. 2003a, *A&A*, 398, 731
- . 2003b, *A&A*, 398, 721
- Tehrany, M. G., Lammer, H., Hanslmeier, A., Ribas, I., Guinan, E. F., & Kolb, C. 2002, poster paper EGS02-A-01903, presented at the European Geophysical Society 22nd General Assembly, <http://www.cosis.net/abstracts/EGS02/01903/EGS02-A-01903.pdf>
- Telleschi, A., Güdel, M., Briggs, K. R., Audard, M., Skinner, S. L., & Ness, J.-U. 2005, *ApJ*, submitted
- Terada, N., et al. 2005, *Icarus*, in press
- Vidal-Madjar, A., Lecavalier des Etangs, A., Désert, J.-M., Ballester, G. E., Ferlet, R., Hébrand, G., & Mayor, M. 2003, *Nature*, 422, 143
- Wichmann, R., Schmitt, J. H. M. M., & Hubrig, S. 2003, *A&A*, 399, 983
- Wood, B. E., & Linsky, J. L. 1997, *ApJ*, 474, L39
- Wood, B. E., Linsky, J. L., Müller, H.-R., Zank, G. P. 2001, *ApJ*, 547, L49
- Wood, B. E., Müller, H.-R., Zank, G., & Linsky, J. L. 2002a, *ApJ*, 574, 412
- Wood, B. E., Redfield, S., Linsky, J. L., Müller, H.-R., & Zank, G. P. 2004, *ApJ*, submitted
- Wood, B. E., Redfield, S., Linsky, J. L., & Sahu, M. S. 2002b, *ApJ*, 581, 1168
- Woods, T. N., Rottman, G. J., Bailey, S. M., Solomon, S. C., & Worden, J. R. 1998, *Sol. Phys.*, 177, 133
- Woods, T. N., Tobiska, W. K., Rottman, G. J., & Worden, J. R. 2000, *J. Geophys. Res.*, 105(A12), 27195
- Zahnle, K. J., & Walker, J. C. G. 1982, *Rev. Geophys. Space Phys.*, 20, 280